Suppression of Transition to Turbulence at High Reynolds Numbers Due to Unsteadiness Imposition

Kazuyoshi Nishihara,* Yusuke Nakahata,† Yoshiaki Ueda,†
Yasushi Sasaki,†† and Manabu Iguchi†

(Dated: June 3, 2010)

Abstract

Transition from laminar to turbulent flow has been a primary concern on the study of a pipe flow. This study provides the analytical solutions of the axisymmetric Navier–Stokes equations for an arbitrary-accelerating laminar flow with a given cross-sectional mean velocity in a circular pipe. The cross-sectional mean velocity is imposed as cubic polynomial with respect to time. The exact solutions obtained are thought to be useful to verify the accuracy of the corresponding experimental results for investigating the transition process to turbulence and, to control the cross-sectional mean velocity in the experiment. Unfortunately, the exact solutions involve the infinite series with respect to the time and the zeros of the second-order usual Bessel function of the first kind. To avoid a difficulty of computing the infinite series for a very small time, this study investigates the asymptotic behavior for the early stage of motion. In addition, a singular perturbation approach is presented in Appendix and the truncation error in computing the infinite series is investigated. As a result, a radial velocity distribution, a pressure gradient and a shear stress are given for four kinds of typical acceleration patterns and compared with the preceding experimental results on the radial velocity distribution. Thickness of the boundary-layer, the pressure gradient and the shear stress are also calculated at a transition point to turbulence using the previous experimentally measured values of a transition time.

PACS numbers: Valid PACS appear here

I. INTRODUCTION

It is of practical importance to save pumping energy in pipeline systems as well. In this study a particular attention is paid to the possibility that imposition of unsteadiness on a pipe flow can control the flow to remain laminar at high Reynolds numbers. Frictional losses in laminar pipe flow are known to be usually much lower than those in turbulent pipe flow. If this possibility is realized, fluid pumping power can be significantly reduced.

Hino *et al.* [1] found based on oscillating pipe flow experiments that temporal acceleration suppresses the transition to turbulence, while temporal deceleration promotes it. The oscillating flow is defined as the flow whose time-averaged value is absent and, hence, the flow direction changes periodically. Later, the same effects were confirmed for a pulsating pipe flow with non-zero time averaged value [2].

An accelerating pipe flow is an intriguing issue on the study of a transition process to turbulence. The pioneering work of the analysis of the accelerating pipe flow can be found in Szymanski [3] who derived the exact solutions of the axisymmetric incompressible Navier–Stokes equations for the pipe flow accelerating with a given pressure gradient. Later, an unsteady pulsating pipe flow has been

sufficiently investigated on laminar and turbulent flow with a careful experiment [4–12]. The analytical solution on the laminar pulsating flow was derived by e.g. Uchida [4] within a small range of the Reynolds number. In contrast to the pulsating flow, an accelerating pipe flow is known to be delay in the transition to turbulence (see e.g., [13–21]), and the transition Reynolds number for a constant-accelerating pipe flow increases monotonically from 2×10^5 to 5×10^5 as the acceleration strongly increases (see the experimental studies of Lefebvre & White [13, 14]). This is because amplification of incoming disturbance is suppred by temporal acceleration. Recent studies on the constant-accelerating pipe flow have focused on a near-wall velocity distribution which relates to an unsteady boundary-layer (see e.g., Greenblatt & Moss [18]; Koppel & Ainola [19]; Das & Arakeri [22, 23]). These results suggest that a suitable periodical imposition of temporal acceleration and deceleration may suppress the transition to turbulence at high Reynolds numbers. In order to examine this possibility it is necessary to generate a pipe flow of arbitrary wave form and derive an analytical solution to it.

Our previous studies have reported that a butterfly valve driven by a stepper motor, which follows pre-programmed rotation speed, can produce an arbitrary-accelerating flow in a brass pipe. The verifications of the system have been done for a constant-accelerating flow in a circular pipe (see Nishihara *et al.* [21]) or a square duct (see Nishihara *et al.* [20]), and two patterns of propagation of turbulence were observed in the experiments. According to the study of Nishihara *et al.* [24], a controlled cross-sectional mean velocity of an arbitrary accelerating flow, which is produced by the system, can be nicely fitted to cubic polynomial with respect to time.

As a first step of the research series, the purpose of this paper is hence to provide the analytical solutions of an accelerating pipe flow whose cross-sectional mean velocity is given by cubic polynomial with respect to time, and to investigate an effect of the initial history of flow started from rest to transition to turbulence. The exact solutions obtained are difficult to handle it for the early stage of motion because of an infinite series involved. The asymptotic behavior at the early stage of motion is therefore investigated and the truncation error in the computation of the infinite series are also presented with the use of a singular perturbation procedure in Appendix. Although the similar singular perturbation approach has been already done for the Hagen–Poiseuille flow by Ghidaoui & Kolyshkin [25], the present findings are thought to be useful to verify the accuracy of the associated experiment for investigating a transition process to turbulence, and of course to dynamically control turbulence for some engineering designs of a circular pipe. Actually, some engineering devices such as a usual pump or blower are known to discharge a liquid or gas into a pipe initially with a cross-sectional mean velocity having not a constant-acceleration but polynomial with respect to time.

II. ANALYSIS
Problem Statement and the Axisymmetric Navier–Stokes Equations

We will deal with a situation where a quiescent incompressible fluid in a circular pipe experiences an acceleration with cubic polynomial velocity and the acceleration is stopped at an elapsed time t_1 (see Fig. 1). The gas flow has the viscosity ν and the density ρ. The resulting flow has the final Reynolds number $\mathrm{Re} = 2u_{m,st}R/\nu$ based on the final constant velocity $u_{m,st}$ for $t \geq t_1$ and the radius of the pipe R. The present analysis targets a laminar flow.

As shown in a series of articles of Ohmi and Iguchi (see e.g., Ohmi *et al.* [12]), the present target flow makes it possible to deal as the axisymmetric. The axisymmetric Navier–Stokes equation in the x-direction is described as

$$\frac{\partial u}{\partial t} = -\frac{1}{\rho}\frac{\partial p}{\partial x} + \nu\left(\frac{\partial^2 u}{\partial r^2} + \frac{1}{r}\frac{\partial u}{\partial r}\right) \tag{1}$$

with a set of initial and boundary conditions

$$u(R;0) = 0, \quad u(R;t) = 0 \quad \text{and} \quad u(0;t) < \infty. \tag{2}$$

Here, u is the velocity and p the pressure. The dimensionless variables are selected as follows:

$$u' = Ru/\nu, \quad x' = x/R, \quad t' = t\nu/R^2, \quad p' = pR^2/(\rho\nu^2), \quad r' = r/R. \tag{3}$$
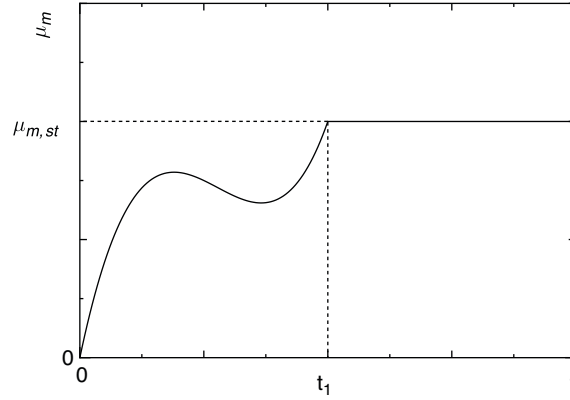
Figure 1: A given cross-sectional mean velocity u_m with cubic polynomial with respect to time: $u_m = a_1 t^3 + a_2 t^2 + a_3 t$ for $0 \leq t \leq t_1$ and $u_m = u_{m,St}$ for $t > t_1$, where a_i ($i = 1, 2, 3$) are real numbers in positive or negative.

In a pipe flow problem the velocity u is usually averaged over the cross-section:

$$\frac{\partial u'_m}{\partial t'} + \frac{\partial p'}{\partial x'} + 2\tau'_w = 0, \tag{4}$$

in which u'_m is the dimensionless mean velocity averaged over the cross-section, i.e., $u'_m = 2\int_0^1 r'u'\mathrm{d}r'$, and τ'_ω is the dimensionless shear stress on the wall $\tau'_\omega = -(\partial u'/\partial r')_{r'=1}$.

Defining the Laplace transform $\widetilde{\mathcal{W}}$ of a function $\mathcal{W}(x',t')$ as

$$\widetilde{\mathcal{W}}(x'; s) = \mathcal{L}\,[\mathcal{W}(x',\,t')] = \int_0^\infty \mathcal{W}(x',\,t')\,\exp\,(-st')\mathrm{d}t' \quad \text{for } s > 0, \tag{5}$$

we obtain $\widetilde{H}(s) = 1/s$ and, since the initial condition of Eq.(2), the Laplace transform of $\partial u'/\partial t'$ deduces to $s\widetilde{u'}$. Accordingly, taking the Laplace transform of Eqs.(1) and (2), one readily obtain the governing equation in dimensionless form as

$$\frac{\partial^2 \widetilde{u}'}{\partial r'^2} + \frac{1}{r'}\frac{\partial \widetilde{u}'}{\partial r'} - s\widetilde{u}' = -\left(-\widetilde{\frac{\partial p'}{\partial x'}}\right). \tag{6}$$

The above differential equation is easily solved using the last two boundary conditions of Eq.(2) (the last constraint of Eq.(2) is required not to make the center-line velocity diverge):

$$\widetilde{u}' = \frac{1}{s}\left(-\widetilde{\frac{\partial p'}{\partial x'}}\right)\left[1 - \frac{J_0(i\sqrt{s}r')}{J_0(i\sqrt{s})}\right], \tag{7}$$

where $i = \sqrt{-1}$ and J_m is the mth-order usual Bessel function of the first kind. Furthermore, averaging Eq.(7) over the cross-section gives

$$\left(-\widetilde{\frac{\partial p'}{\partial x'}}\right) = -\frac{sJ_0(i\sqrt{s})}{J_2(i\sqrt{s})}\widetilde{u}'_m. \tag{8}$$

Substituting Eq.(8) into Eq.(7), we finally have the exact solution to Eq.(1)

$$\widetilde{u}' = \left[\frac{J_0(i\sqrt{s}r')}{J_2(i\sqrt{s})} - \frac{J_0(i\sqrt{s})}{J_2(i\sqrt{s})}\right]\widetilde{u}'_m. \tag{9}$$

Exact Solution to Accelerating Flow with Cubic Mean Velocity Pattern

We deal with an accelerating flow whose cross-sectional mean velocity is given by the cubic polynomial, i.e.,

$$u'_m(t) = \begin{cases} a_1 t'^3 + a_2 t'^2 + a_3 t' & \text{for } 0 \le t' \le t'_1, \\ u'_{m,st} & \text{for } t' > t'_1. \end{cases} \tag{10}$$

Note that the coefficients a_1, a_2 and a_3 are respectively a real number in positive or negative and the mean velocity $u'_m(t')$ matches at $t' = t'_1$, i.e., $u'_{m,st} = a_1 t'^3_1 + a_2 t'^2_1 + a_3 t'_1$. The solution of the problem can be obtained by substituting the Laplace transformed $u'_m(t')$ into Eq.(9) and then taking the inverse Laplace transform.

The Laplace transform of the given mean velocity (10), i.e., $\widetilde{u'_m} = \int_0^{t'_1} \left(a_1 t'^3 + a_2 t'^2 + a_3 t' \right) e$

$xp\left(-st'\right) dt' + \int_{t'_1}^{\infty} u'_{m,st} \exp(-st') dt'$ is readily calculated using the integration by parts:

$$\widetilde{u}'_m = -(3a_1 t'^2_1 + 2a_2 t'_1 + a_3) \frac{e^{-st'_1}}{s^2} - (6a_1 t'_1 + 2a_2) \frac{e^{-st'_1}}{s^3} - 6a_1 \frac{e^{-st'_1}}{s^4} + \frac{a_3}{s^2} + \frac{2a_2}{s^3} + \frac{6a_1}{s^4} \quad . \tag{11}$$

Substituting Eq.(ll) into Eq.(9), we have

$$\widetilde{u}' = \left[\frac{J_0(i\sqrt{s}r')}{J_2(i\sqrt{s})} - \frac{J_0(i\sqrt{s})}{J_2(i\sqrt{s})} \right] \left\{ -(3a_1 t'^2_1 + 2a_2 t'_1 + a_3) \frac{e^{-st'_1}}{s^2} - (6a_1 t'_1 + 2a_2) \frac{e^{-st'_1}}{s^3} \right.$$

$$\left. - 6a_1 \frac{e^{-st'_1}}{s^4} + \frac{a_3}{s^2} + \frac{2a_2}{s^3} + \frac{6a_1}{s^4} \right\} . \tag{12}$$

To obtain the inverse Laplace transform of Eq.(12), the residue at the singular points of Eq.(12) is needed to calculate. When the zeros of $I_2(i\sqrt{s})$ are defined as s_n (note that $i\sqrt{s_n} := y_n \neq 0$ for $n \ge 1$), $I_2(i\sqrt{s})$ behaves near $s = s_n$ like $J_2(i\sqrt{s}) = \left| (d/ds)J_2(i\sqrt{s}) \right|_{s=s_n} (s - s_n) + \cdots$ in which the derivative of $I_2(i\sqrt{s})$ is calculated using the well-known formula of $(d/dy)J_2(y) = J_1(y) - (2/y)J_2(y)$. Then, the required residue, Res, at $s = s_n$ is respectively calculated as

$$G^n_m (r'; t') := \text{Res}_{s=s_n} \left[\left\{ \frac{J_0(i\sqrt{s}r')}{J_2(i\sqrt{s})} - \frac{J_0(i\sqrt{s})}{J_2(i\sqrt{s})} \right\} \frac{e^{st'}}{s^m} \right]$$

$$= (-1)^m \frac{4 \exp(-y^2_n t')}{y^{2m}_n J_0(y_n)} (J_0(y_n) - J_0(y_n r')) \quad \text{for } m = 2, 3, 4. \tag{13}$$

Here, the zeros y_n are obtained from the formula 9.5.12 of Abramowitz & Stegun [26]. The unsteady solution to Eq.(12) recovers from the Laplace space using the inverse Laplace transform defined by

$$\mathcal{W}(t') = \mathcal{L}^{-1}[\widetilde{\mathcal{W}}(s)] = \frac{1}{2\pi i} \int_{c-i\infty}^{c+i\infty} \widetilde{\mathcal{W}}(s) \exp(st') ds. \tag{14}$$

To calculate the integral, one takes the contour L_1, shown in Fig. 2, which consists of the real axis from 0 to $-\infty$. Changing the variable s to $s = \varepsilon \exp(i\theta)$, the integral range of $\mathcal{L}^{-1}[\widetilde{u}'(s)]$ is divided into $\int_{\infty \exp(-i\pi)}^{\delta}(-d\varepsilon) + \int_{\delta}^{\infty \exp(-i\pi)}(-d\varepsilon) + \int_{-\pi}^{\pi} d\varepsilon + \sum_n \text{Res}_{s_n}$ in which the first two terms cancel each other. We then consider the third integral $\int_{-\pi}^{\pi} d\varepsilon$, defined as $W_m(r'; t')$ with the order of pole m at the origin, of the term having the pole of the highest order at the origin in Eq.(12), i.e., $[J_0(i\sqrt{s}r')/J_2(i\sqrt{s}) - J_0(i\sqrt{s}r')/J_2(i\sqrt{s})]/s^4$. Then, the third integral $W_4(r'; t')$ is written as

$$W_4(r'; t') = \frac{1}{2\pi} \int_{-\pi}^{\pi} \frac{1}{\varepsilon^2 e^{2i\theta}} \frac{J_0\left(i\sqrt{\varepsilon}e^{i\theta/2}r'\right) - J_0\left(i\sqrt{\varepsilon}e^{i\theta/2}\right)}{J_2\left(i\sqrt{\varepsilon}e^{i\theta/2}\right)} \exp\left(\varepsilon t' e^{i\theta}\right) d\theta. \tag{15}$$
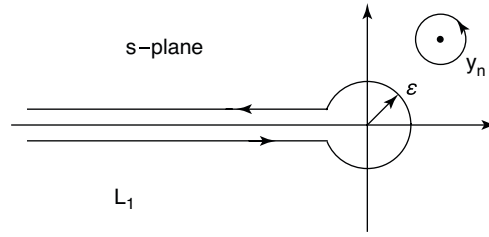
Figure 2: Integral contour L_1.

For $\varepsilon \ll 1$, the Bessel function is expanded into the ascending power series (see the formula 9.1.10 of Abramowitz & Stegun [26])

$$J_n(z) = \left(\frac{z}{2}\right)^n \sum_{k=0}^{\infty} \frac{\left(-z^2/4\right)^k}{k!\,\Gamma(n+k+1)}, \tag{16}$$

where Γ is the Gamma function defined by $\Gamma(z) = \int_0^{\infty} w^{z-1} \exp(-w)\mathrm{d}w$. As will be discussed below, the calculation of Eq.(15) requires the terms of Eq.(16) within the fourth order so that the summation of Eq.(16) truncates at $k = 4$. Substituting Eq.(16) into Eq.(15) gives

$$W_4(r';t') = \frac{1}{2\pi}\int_{-\pi}^{\pi} \frac{1}{\varepsilon^3 e^{3i\theta}} \frac{\frac{1}{4}\varepsilon e^{i\theta}\left(r'^2-1\right) + \frac{1}{64}\varepsilon^2 e^{2i\theta}\left(r'^4-1\right) + \frac{1}{2304}\varepsilon^3 e^{3i\theta}\left(r'^6-1\right) + \frac{1}{147456}\varepsilon^4 e^{4i\theta}\left(r'^8-1\right)}{-\frac{1}{8}\varepsilon e^{i\theta}\left(1 + \frac{1}{12}\varepsilon e^{i\theta} + \frac{1}{384}\varepsilon^2 e^{2i\theta} + \frac{1}{23040}\varepsilon^3 e^{3i\theta}\right)}$$
$$\times \left(1 + \varepsilon e^{i\theta}t' + \frac{1}{2}\varepsilon^2 e^{2i\theta}t'^2 + \frac{1}{6}\varepsilon^3 e^{3i\theta}t'^3 + \frac{1}{24}\varepsilon^4 e^{4i\theta}t'^4\right)\mathrm{d}\theta. \tag{17}$$

Taking into account that $(1 + a\varepsilon + b\varepsilon^2 + c\varepsilon^3)^{-1} \approx 1 - a\varepsilon + (a^2-6)\varepsilon^2 + (-a^3+2ab-c)\varepsilon^3$ for $\varepsilon \ll 1$, Eq.(17) becomes (using the approximation to the denominator of Eq.(17))

$$W_4(r';t') = \frac{1}{2\pi}\int_{-\pi}^{\pi} \frac{8}{\varepsilon^4 e^{4i\theta}}\left[\frac{1}{4}\varepsilon e^{i\theta}\left(1-r'^2\right) + \frac{1}{64}\varepsilon^2 e^{2i\theta}\left(1-r'^4\right) + \frac{1}{2304}\varepsilon^4 e^{3i\theta}\left(1-r'^6\right)\right.$$
$$\left. + \frac{1}{147456}\varepsilon^4 e^{4i\theta}\left(1-r'^8\right)\right]\left(1 + \varepsilon e^{i\theta}t' + \frac{1}{2}\varepsilon^2 e^{2i\theta}t'^2 + \frac{1}{6}\varepsilon^3 e^{3i\theta}t'^3\right)$$
$$\times \left(1 - \frac{1}{12}\varepsilon e^{i\theta} + \frac{5}{1152}\varepsilon^2 e^{2i\theta} - \frac{351}{1866240}\varepsilon^3 e^{3i\theta}\right)\mathrm{d}\theta. \tag{18}$$

In the calculation of Eq.(18), the integrand holds the terms being independent of $\varepsilon e^{i\theta}$. Therefore, we have

$$W_4(r';t') = \frac{1}{3}\left(1-r'^2\right)\left(t'^3 - \frac{1}{4}t'^2 + \frac{5}{192}t' - \frac{351}{311040}\right) + \frac{1}{16}\left(1-r'^4\right)\left(t'^2 - \frac{1}{6}t' + \frac{5}{576}\right)$$
$$+ \frac{1}{288}\left(1-r'^6\right)\left(t' - \frac{1}{12}\right) + \frac{1}{18432}\left(1-r'^8\right). \tag{19}$$

To obtain the inverse Laplace transform of Eq.(12), we furthermore need to calculate W_2 and W_3. Similar to W_4, the calculation of W_2 and W_3 are respectively performed within the order of $k = 2$ and $k = 3$ in Eq.(16).

$$W_2(r';t') = 2(1-r'^2)t' - \frac{1}{24}(1-r'^2)(1-3r'^2), \tag{20}$$

$$W_3(r';t') = (1-r'^2)\left(t'^2 - \frac{1}{6}t' + \frac{5}{576}\right) + \frac{1}{8}(1-r'^4)\left(t' - \frac{1}{12}\right) + \frac{1}{288}(1-r'^6). \tag{21}$$

Finally, taking into account that the well-known formula $\mathcal{L}[H(t'-t_1')f(t'-t_1')] = \exp(-t_1's)\widetilde{f(s)}$, and substituting Eqs.(13) and (19)—(21) into Eq.(12), the exact solution $u'(r';t')$ is obtained as

$$u'(r';t') = a_3 Z_2(r';t') + 2a_2 Z_3(r';t') + 6a_1 Z_4(r';t') - H(t'-t_1')\big[(3a_1 t_1'^2 + 2a_2 t_1' + a_3)$$

$$\times Z_2(r'; t'-t_1') + (6a_1 t_1' + 2a_2)Z_3(r'; t'-t_1') + 6a_1 Z_4(r'; t'-t_1')\big] \tag{22}$$

with

$$Z_m(r';t') := \left[W_m(r';t') + \sum_{n=1}^{\infty} G_m^n(r';t') \right]. \tag{23}$$

Similarly, the pressure gradient can be also obtained using Eq.(8) as

$$-\frac{dp'}{dx'} = a_3 \overline{Z}_1(t') + 2a_2 \overline{Z}_2(t') + 6a_1 \overline{Z}_3(t') - H(t'-t_1')\big[(3a_1 t_1'^2 + 2a_2 t_1' + a_3)$$

$$\times \overline{Z}_1(t'-t_1') + (6a_1 t_1' + 2a_2)\overline{Z}_2(t'-t_1') + 6a_1 \overline{Z}_3(t'-t_1')\big], \tag{24}$$

where

$$\overline{Z}_m(t') := \left[\overline{W}_m(t') - \sum_{n=1}^{\infty} \overline{G}_m^n(t') \right] \tag{25}$$

with

$$\overline{W}_1(t') := 8t' + \frac{4}{3}, \tag{26}$$

$$\overline{W}_2(t') := 4t'^2 + \frac{4}{3}t' - \frac{1}{144}, \tag{27}$$

$$\overline{W}_3(t') := \frac{4}{3}t'^3 + \frac{2}{3}t'^2 - \frac{1}{144}t' + \frac{1}{4320}, \tag{28}$$

$$\overline{G}_m^n(t') := (-1)^{m+1}\frac{4\exp(-y_n^2 t')}{y_n^{2m}} \qquad \text{for } m = 1, 2, 3. \tag{29}$$

The shear stress is easily obtained from Eq.(4) with Eqs.(l0) and (24).

Asymptotic Behavior at the Early Stage of Motion

The exact solutions obtained in §§IIB involve the infinite series with respect to the time and the zeros y_n (see the second terms of Eqs.(23) and (25)). In the actual computation of the infinite series in Eqs.(22) and (24), the computation need to truncate within a finite n. For $t' \ll 1$, the zeros y_n are required up to a sufficient high order to converge the computation. Instead, this subsection investigates the asymptotic behavior of Eq.(12) for $s \gg 1$ with $r' \gg s^{-1/2}$ and then takes the inverse Laplace transform to obtain the initial behavior in the real space. Note that we present a singular perturbation approach for the early stage of motion in Appendix.

For $s \gg 1$, Eq.(12) behaves like

$$\tilde{u}'(r') \sim \left\{ 1 - \frac{1}{\sqrt{r'}}\exp\big[\sqrt{s}(r'-1)\big] \right\}\left(\frac{a_3}{s^2} + \frac{2a_2}{s^3} + \frac{6a_1}{s^4} \right). \tag{30}$$

Here, we used the relations of $J_0(iz) \sim (i\pi z)^{-1/2}(\cosh z - i\sinh z)$ and $J_2(iz) \sim -(i\pi z)^{-1/2}(\cosh z - i\sinh z)$ which are obtained from the asymptotic expansion $J_n(z) \sim [2/(\pi z)]^{1/2}\cos(z - [(2n+1)_\pi]/4)$.

To investigate the feature of the flow near the wall (inside the boundary-layer), we introduce a small variable $r' := (1 - \bar{r}') \ll 1$ with $s^{1/2}\bar{r}' \ll 1$. Then, Eq.(30) approximately reduces to

$$\tilde{u}'(\bar{r}') \sim s^{1/2}\left(\frac{a_3}{s^2} + \frac{2a_2}{s^3} + \frac{6a_1}{s^4} \right)\bar{r}'. \tag{31}$$

Using the well-known formula of the inverse Laplace transform $\mathcal{L}^{-1}[\Gamma(c)/(s - \alpha)^c] = t^{c-1} \exp(\alpha t')$ with the real part of c being positive, we obtain

$$u'(\bar{r}'; t') \approx \frac{1}{\sqrt{\pi}}\left[\frac{16}{5}a_1t'^{5/2} + \frac{8}{3}a_2t'^{3/2} + 2a_3t'^{1/2}\right]\bar{r}' \qquad \text{for } t' \ll 1. \tag{32}$$

The shear stress is readily calculated from $\tau'_w = \mathrm{d}u'/\mathrm{d}\bar{r}'$ at $\bar{r}' = 0$:

$$\tau'_w(t') \approx \frac{1}{\sqrt{\pi}}\left[\frac{16}{5}a_1t'^{5/2} + \frac{8}{3}a_2t'^{3/2} + 2a_3t'^{1/2}\right] \qquad \text{for } t' \ll 1. \tag{33}$$

Also, the initial pressure gradient, $-\mathrm{d}p'/\mathrm{d}x'$, is obtained from Eq.(4) as

$$-\frac{\mathrm{d}p'}{\mathrm{d}x'} \approx (3a_1t'^2 + 2a_2t' + a_3) + \frac{2}{\sqrt{\pi}}\left(\frac{16}{5}a_1t'^{5/2} + \frac{8}{3}a_2t'^{3/2} + 2a_3t'^{1/2}\right) \qquad \text{for } t' \ll 1. \tag{34}$$

The first term is the contribution from $\mathrm{d}u'_m/\mathrm{d}t'$, and the second term is from τ'_w. At the early stage of motion, the pressure gradient is found to be dominantly affected from $\mathrm{d}u'_m/\mathrm{d}t'$ rather than τ'_w.

The thickness of the boundary-layer δ', which is here defined by $u' = 0.99u'_m$, is determined fulfilling the following equation:

$$\frac{1}{\sqrt{\pi}}\left[\frac{16}{5}a_1t'^{5/2} + \frac{8}{3}a_2t'^{3/2} + 2a_3t'^{1/2}\right]\delta' = 0.99(a_1t'^3 + a_2t'^2 + a_3t') \tag{35}$$

which leads to $\delta' \approx 0.495\pi^{1/2} (a_1/a_3)t'^{1/2}$ for $t' \ll 1$ for all the patterns of acceleration with a_1, a_2 and a_3 having nonzero values.

III. DISCUSSION
Test Case: Linearly Accelerating Flow
To verify the analysis we investigate a linearly accelerating flow in which the mean velocity is set at $a_1 = a_2 = 0$ with $a_3 > 0$. This flow has been already analysed and compared with the experimental results by e.g., Nishihara et al. [21]. Setting $a_1 = a_2 = 0$ in Eq.(22), the velocity (22) reduces to

$$u'(r'; t') = a_3 [Z_2(r'; t') - H(t' - t'_1)Z_2(r'; t' - t'_1)] \tag{36}$$

in which Eqs.(13), (20) and (23) hold. Then, Eq.(36) is found to agree perfectly with the previous analytical solutions of Das & Arakeri [23] (see Eqs.(27) and (28) of their paper) and Nishihara et al. [21] (see Eq.(19) of their paper) in which t'_1 is replaced by $u'_{m,st}/a_3$. This flow pattern is again investigated in the following subsection together with some kinds of acceleration patterns having nonzero values of a_1 and a_2.

Arbitrary Accelerating Flow
This subsection considers an accelerating flow which is produced by Eq.(10).

1. Comparison with the preceding experimental results on the radial velocity distribution
To compare with the associated experimental results of Nishihara et al. [24], we here select the following three kinds of acceleration patterns (see Fig. 3) including the linear acceleration pattern shown in §§IIIA:
   (A) $a_1 = 6, 302, 385, 797$, $a_2 = -142, 212, 942$, $a_3 = 1, 741, 065$
   (B) $a_1 = 0$, $a_2 = 0$, $a_3 = 913, 952$
   (C) $a_1 = 8, 010, 953, 445$, $a_2 = -39, 556, 131$, $a_3 = 481, 793$.
These coefficients are determined from the given mean velocity patterns with $t'_1 = 0.0105$ in the associated experiments of Nishihara et al. [24], i.e., the coefficients are determined by the least-square fitting of the measured values which are shown in Fig. 3 as circle, triangle and square dots. Note that the coefficients a_1, a_2 and a_3 exhibit the very large values due to the dimensionless procedure. For reference, the following experimentally measured values at 4,000 mm (= 102.56R) from the inlet are
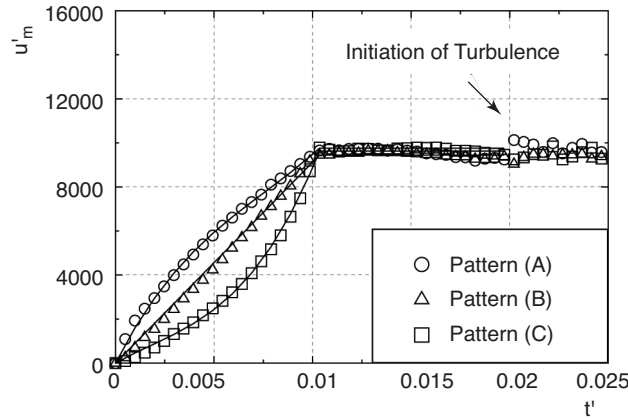
Figure 3: Given cross-sectional mean velocities in (dots): associated experiment of Nishihara *et al.* [24] for patterns (A), (B) and (C) together with (solid lines): the analytical results which are calculated from $u'_m = 2\int_0^1 r'u'dr'$.

listed in Table 1; t_{tr}: initiation time of turbulence, t_i: acceleration imposition period, T_{lag}: time lag, $u_{m,st}$: cross-sectional mean velocity of the final steady pipe flow, Re: the Reynolds number.

Table 1: Measured values at $x = 4,000$ mm (= 102.56R) from the inlet.

	Pattern (A)	**Pattern (B)**	**Pattern (C)**
t_{tr} (s)	1.93	2.00	2.04
t_i (s)	1.05	1.05	1.05
T_{lag} (s)	0.88	0.95	0.99
$u_{m,st}$ (m/s)	3.69	3.64	3.68
Re(−)	19,200	18,900	19,100

The calculation of the cross-sectional mean velocity u'_m from Eq.(22) returns to the given velocity patterns (A) to (C). This makes it possible to verify the accuracy of computing the infinite series related to $G_m^n (r'; t')$. As mentioned above, the mean velocity u'_m can be analytically calculated from $u'_m = 2\int_0^1 r'u' dr'$. Instead of the analytical calculation which requires a cumbersome task, the mean velocity u'_m is here computed using a trapezoidal quadrature with the twenty base points distributed within the closed interval [0,1]. In addition, the zeros y_n needed in computing the infinite series of Eq.(23) (i.e., Eq.(13)) are adopted up to the first one-hundred points, $y_1, y_2, \cdots, y_{100}$ to converge the computation for very small time [28] (see Fig. 6). As shown in Fig. 3 (analytical results are depicted in solid lines), the mean velocity u'_m is recovered from Eq.(22), and hence the present analysis is found to be valid.

Figure 4 shows the analytical results of the radial velocity distribution (solid line) together with the previous experimental results of Nishihara *et al.* [24] at $x = 102.56R$ from the inlet for patterns (A), (B) and (C) at the various times. The position measured locates behind the entrance region in the experimental condition. As shown in Fig. 4, the present analytical solution is in good agreement with the experimental results.

2. Analytical results for typical kinds of acceleration patterns
Besides patterns (A) to (C), this subsection takes the following pattern (D) which could behave like a combination of a constant-acceleration and a pulsation (see Fig. 5):

(D) $a_1 = 48,141, 585, 042.603$, $a_2 = −842, 807, 085.492317$, $a_3 = 4, 426, 644.27095313$.

The values of $u'_{m,st}$ in pattern (D) (see Eq.(10)) is the same as the ones of patterns (A) to (C).

As mentioned in §§IIC, much attention should be paid for treating the infinite series involved in the exact solution of Eq.(22). Figure 6 shows the near-wall velocity distributions at $t' = 10^{-4}$. The solid lines indicate the exact solution of Eq.(22) within $n = 10$, $n = 20$ or $n = 100$ truncation for computing the infinite series, the dashed lines are the inner and outer asymptotic solutions of Eqs.(Al3) and (A17)
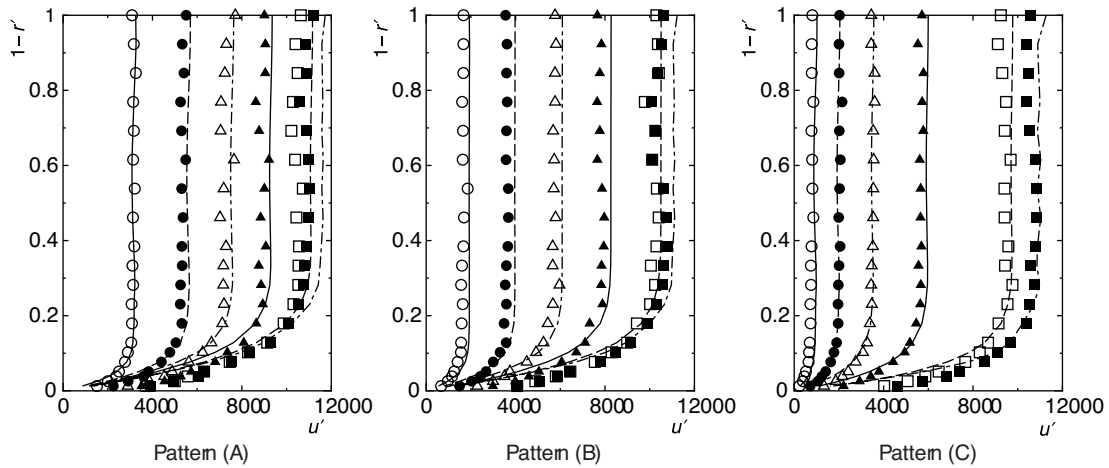
Figure 4: Comparison of unsteady velocity distributions for patterns (A), (B) and (C) at various elapsed time between (lines): the present analytical solution and (dots): the associated experimental results of Nishihara *et al.* [24] at $x = 102.56R$ from the inlet. (○): $t' = 0.002$, (●): $t' = 0.004$, (△): $t' = 0.006$, (▲): $t' = 0.008$, (□): $t' = 0.010$, (■): $t' = 0.0105$.
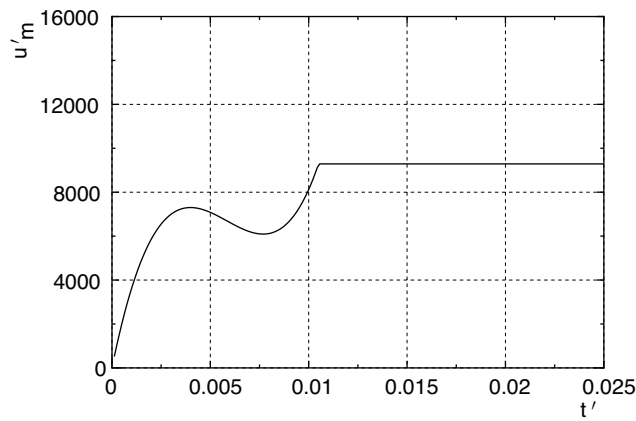

Figure 5: A given cross-sectional mean velocity of pattern (D).

obtained in Appendix, and the dotted line is the asymptotic solution of Eq.(32). As shown in Fig. 6, the computation of the infinite series does not converge within a small number of n at the early stage of motion, while the computation adopting up to $n = 100$ is in excellent agreement with the present asymptotic solutions. As observed in Fig. 6, it can be found that the adoption of y_n within $n = 100$ is sufficient for the computation of the infinite series for $t' \gtrsim O(10^{-4})$. Figure 7 shows the comparison of the initial pressure gradient $-\mathrm{d}p'/\mathrm{d}x'$ for patterns (A) to (D) between the exact solution and the asymptotic behavior of Eq.(34). The asymptotic behavior is seen to be in excellent agreement with the exact solution adopting the zeros y_n up to $n = 100$ because the contribution from $\mathrm{d}u'_m/\mathrm{d}t'$ is dominant for the initial pressure gradient. Of particular interests are that the flow in pattern (D) experiences a negative pressure gradient during $0.004 \lesssim t' \lesssim 0.007$ and the flow in pattern (B) exhibits almost a constant pressure gradient. Figure 8 also shows the comparison of the initial shear stress between the exact solution and the asymptotic behavior of Eq.(33). In contrast to the pressure gradient, a marginal difference is seen in the initial shear stress although there is almost no difference between the two for a very early stage of motion.

Figure 9 shows the velocity distributions u' for patterns (A) to (D) at different times. As shown in Table 2, the transition to turbulence was observed around $t' \approx 0.02$ in the preceding experiment for patterns (A) to (C). For reference, we list in Table 2 the thickness of boundary-layer fulfilling
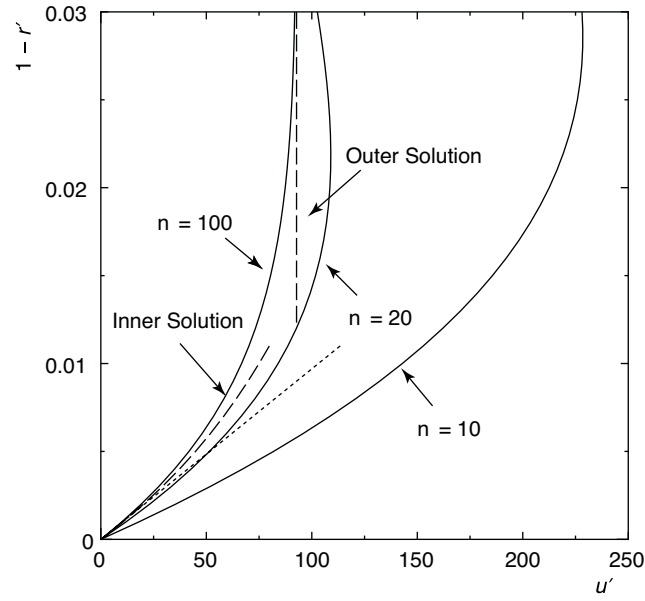
Figure 6: Comparison of the near-wall velocity distribution for pattern (B) at $t' = 10^{-4}$ between (solid): the exact solution of Eq.(22) within $n = 10$, $n = 20$ or $n = 100$ truncation and (dashed): the asymptotic inner and outer solutions of Eqs.(A13) and (A17) together with (dotted): the asymptotic solution of Eq.(32).
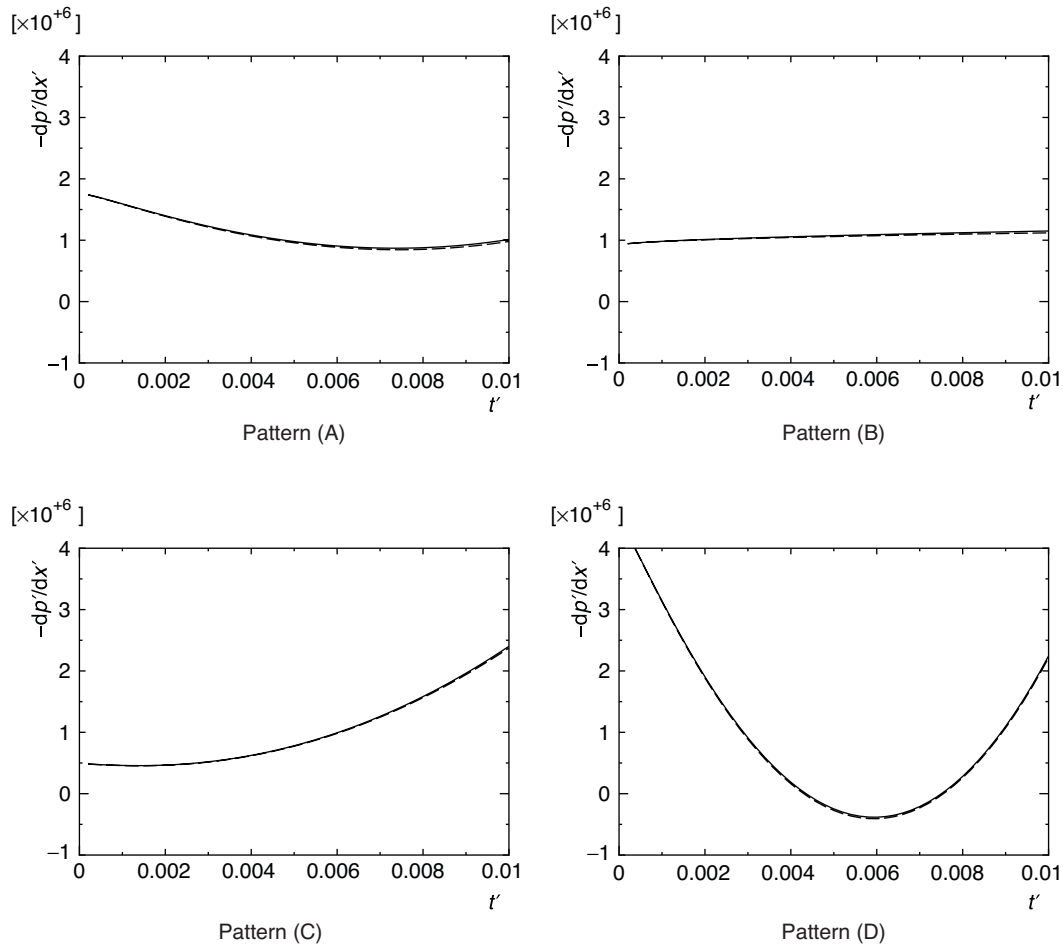

Figure 7: Comparison of the pressure gradient $-dp'/dx'$ at the early stage of motion between (solid): the exact solution of Eq.(24) and (dashed): the asymptotic solution of Eq.(34).
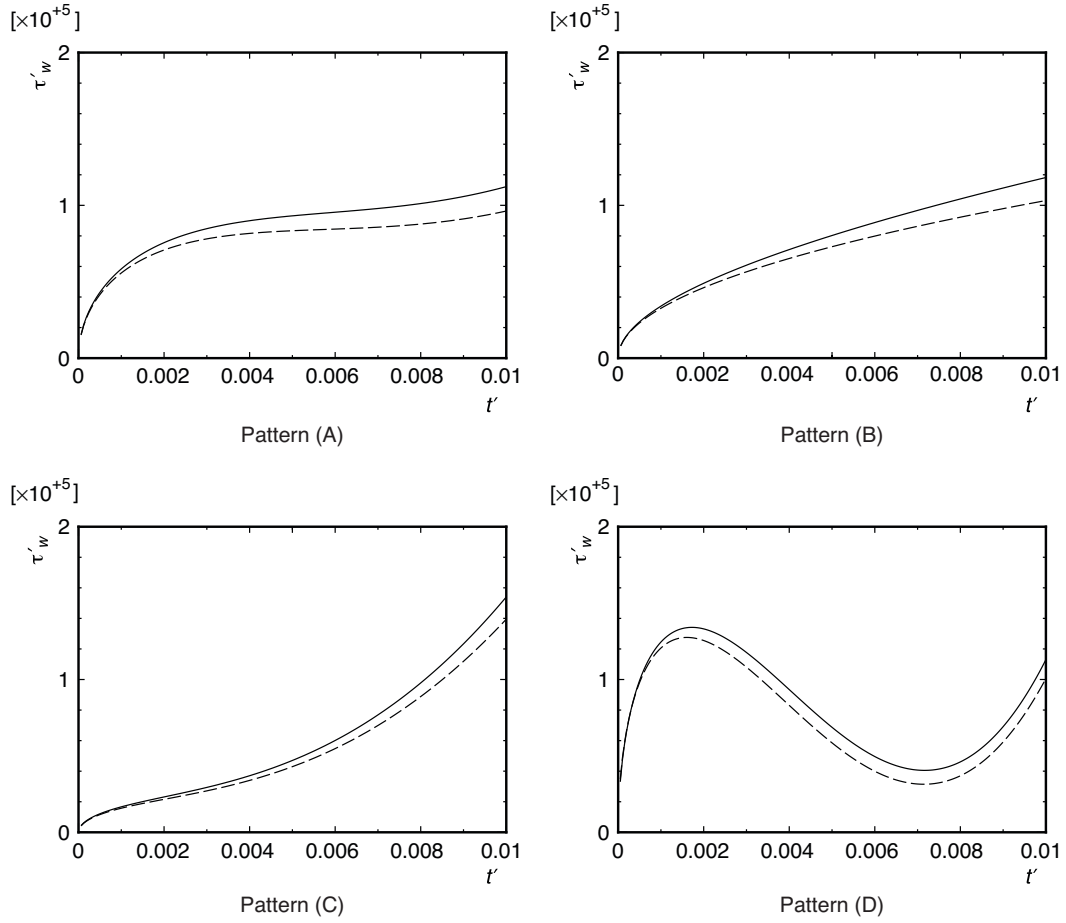
Figure 8: Comparison of the shear stress at the early stage of motion between (solid): the exact solution and (dashed): the asymptotic solution of Eq.(33).

$u'(1 - \delta; t'_{tr}) = 0.99u'/(0; t'_{tr})$, the pressure gradient and the shear stress at the transition point to turbulence, which are calculated by using the experimentally measured initiation time of turbulence (see Table 1 or 2). In Fig. 9, the laminar analytical results at $t' = 0.1$, although it already becomes turbulent flow, are shown to compare with the steady Hagen–Poiseuille flow: $u'(r') = 2u'_m(1 - r'^2)$. Figure 10 shows the pressure gradient of Eq.(24), in which the infinite series involved is computed within $n = 100$, for patterns (A) to (D). At around $t' = t'_1$, the pressure gradient rapidly drops and thereafter approaches to the usual steady laminar pressure drop of a circular pipe: $\Delta p = \lambda[\Delta x/(2R)][u_m^2/(2g)]\rho g$ with $\lambda = 64/Re$. Figure 11 shows the shear stress, which is readily calculated from Eq.(4) with Eq.(24), for patterns (A) to (D). As seen in Figs. 10 and 11, the pressure gradient or the shear stress experiences a similar feature in all the patterns after $t' \approx t'_1$, although exhibiting the quite different in each pattern before $t' \approx t'_1$.

The present analytical solutions can provide a fundamental information on an unsteady flow caused by an acceleration with a cross-sectional mean velocity which is approximately described as cubic polynomial with respect to time. As mentioned in Introduction, the present solutions are useful for a design of a circular pipe to dynamically control turbulence because a usual pump or blower discharges a liquid or gas into a pipe initially with a cross-sectional mean velocity having not a linear but polynomial acceleration with respect to time.

IV. CONCLUDING REMARKS

This study has provided the analytical solutions to the axisymmetric Navier–Stokes equations for an accelerating pipe flow with a given cross-sectional mean velocity having cubic polynomial acceleration with respect to time. The analytical solutions were also verified against the associated experimental
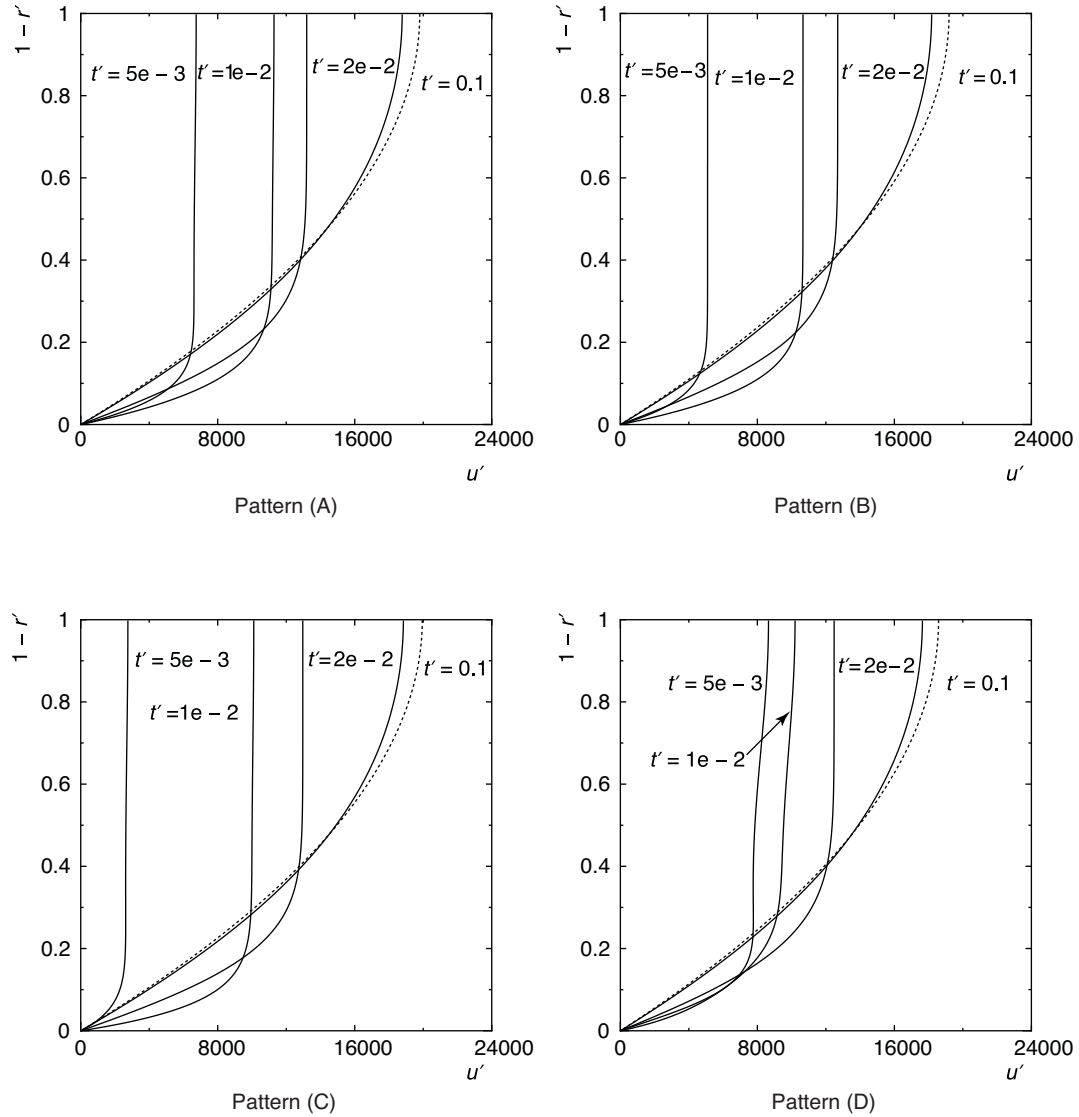
Figure 9: Unsteady velocity distributions for patterns (A), (B), (C) and (D) at different times. The velocity distribution of the steady Hagen–Poiseuille flow is depicted as the dotted line.

Table 2: Thickness of boundary-layer fulfilling $u'(I - \delta'; t'_{tr}) = 0.99u'(0; t'_{tr})$, pressure gradient and shear stress at a transition point to turbulence.

	Pattern (A)	**Pattern (B)**	**Pattern (C)**
Re	19,200	18,900	19,100
t'_{tr}	0.01903353	0.019723865	0.020118343
δ'	0.460	0.458	0.436
$-dp'/dx'$	129,488.843	125,770.18	134,797.671
τ_w^1	64,744.4215	62,885.0898	67,398.8354

results on the radial velocity distributions by Nishihara *ei al.* [24]. The exact solutions involve an infinite series with respect to the time and the zeros of the second-order usual Bessel function of the first kind. This makes it difficult to deal with an initial behavior of the solutions for $t' \ll 1$. To avoid the difficulty of computing the infinite series, we investigated the asymptotic behavior of the flow at the early stage of motion. In addition, the truncation error in computing the infinite series was investigated for $t' \ll 1$ with the use of a singular perturbation approach presented in Appendix. The
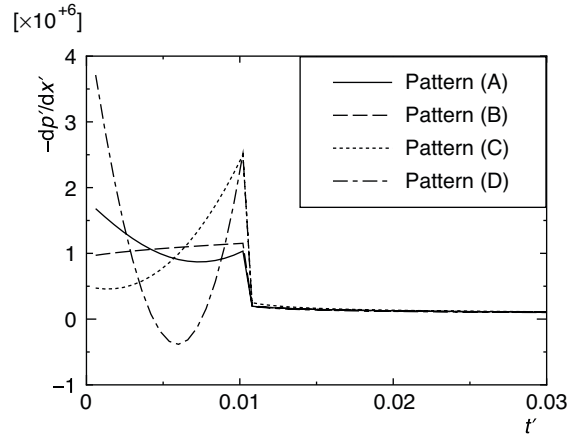
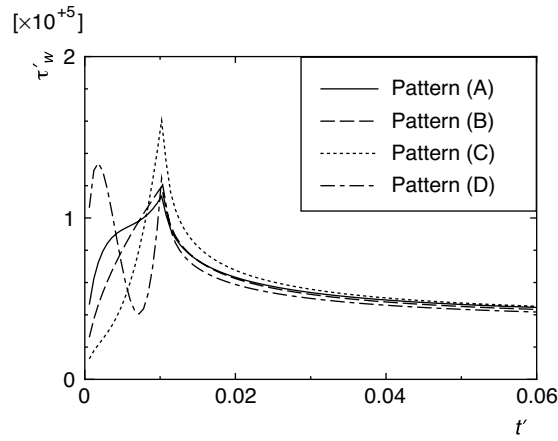**Figure 10:** Pressure gradient $-dp'/dx'$ for patterns (A), (B), (C) and (D).

Figure 11: Shear stress τ'_w for patterns (A), (B), (C) and (D).

thickness of the boundary-layer, the pressure gradient and the shear stress were calculated at a transition point to turbulence using the previous experimentally measured values of the transition time.

The solutions obtained in this study can be used to verify the accuracy of the associated experimental results for investigating a transition process to turbulence and to design a circular pipe in some engineering plants for a dynamic control of turbulence. Actually, a usual pump or blower is known to discharge a liquid or gas into a pipe initially with a cross-sectional mean velocity having not a linear but polynomial acceleration with respect to time. In addition, the present results may suggest that a suitable periodical imposition of temporal acceleration and deceleration suppress the transition to turbulence at high Reynolds numbers.

APPENDIX A: SINGULAR PERTURBATION APPROACH FOR THE EARLY STAGE OF MOTION

This section deals with the flow behavior at the early stage of motion on the basis of the singular perturbation method [27]. This analytical technique is quite suitable for investigating the dominant feature of the flow. The problem setting follows §§IIA. Again, the governing equations are descried as

$$\frac{\partial u'}{\partial t'} = -\frac{\partial p'}{\partial x'} + \left(\frac{\partial^2 u'}{\partial r'^2} + \frac{1}{r'} \frac{\partial u'}{\partial r'} \right), \tag{A1}$$

$$\frac{\partial u'_m}{\partial t'} + \frac{\partial p'}{\partial x'} + 2\tau'_w = 0, \quad \tau'_w = -\left(\frac{\partial u'}{\partial r'} \right)_{r'=1} \tag{A2}$$

with the initial and boundary conditions of

$$u'(r'; +0) = u'_m \quad \text{and} \quad u'(1; t') = 0 \tag{A3}$$

To investigate the flow behavior at the early stage of motion, we introduce the inner variable $\hat{t} = t'/\varepsilon$ with $\varepsilon \ll 1$. Then, Eqs.(Al) and (A2) are respectively written as

$$\frac{\partial u'}{\partial \hat{t}'} = -\varepsilon \frac{\partial p'}{\partial x'} + \varepsilon \left(\frac{\partial^2 u'}{\partial r'^2} + \frac{1}{r'} \frac{\partial u'}{\partial r'} \right), \tag{A4}$$

$$\frac{\partial u'_m}{\partial \hat{t}'} + \varepsilon \frac{\partial p'}{\partial x'} + 2\varepsilon \tau'_w = 0. \tag{A5}$$

Erasing the pressure term between Eqs.(A4) and (A5) gives

$$\frac{\partial u'}{\partial \hat{t}'} = \frac{\partial u'_m}{\partial \hat{t}'} + 2\varepsilon \tau'_w + \varepsilon \left(\frac{\partial^2 u'}{\partial r'^2} + \frac{1}{r'} \frac{\partial u'}{\partial r'} \right). \tag{A6}$$

This equation makes us introduce the inner variable $\hat{r} = (1 - r')/\varepsilon^{1/2}$ to balance the order. In the inner domain, we assume the inner expansion of u' as $u'^i = \sum_{n \geq 0} \varepsilon^{n/2} u'^i_n$, and substitute it into Eq.(A6):

$$\sum_{n \geq 0} \varepsilon^{n/2} \frac{\partial u'^i_n}{\partial \hat{t}'} = \frac{\partial u'_m}{\partial \hat{t}'} + 2\varepsilon \tau'_w + \left[\sum_{n \geq 0} \varepsilon^{n/2} \frac{\partial^2 u'^i_n}{\partial \hat{r}'^2} + \varepsilon^{1/2} (1 + \varepsilon^{1/2} \hat{r}') \sum_{n \geq 0} \varepsilon^{n/2} \frac{\partial u'^i_n}{\partial \hat{r}'} \right]. \tag{A7}$$

Equation (A7) yields the first-order approximation, noting that $\partial^2 u'_m / \partial \hat{r}^2 = 0$, as

$$\frac{\partial}{\partial \hat{t}'} (u'^i_0 - u'_m) = \frac{\partial^2}{\partial \hat{r}^2} (u'^i_0 - u'_m). \tag{A8}$$

This equation represents the so-called heat equation and is readily solved, using the Laplace transform, with the initial and boundary conditions of Eq.(A3) as

$$\tilde{u}'^i_0 = \tilde{u}'_m \left[1 - \exp(-\sqrt{s}\hat{r}') \right]. \tag{A9}$$

The shear stress is calculated from the gradient of the inner velocity at the wall, and thus the first-order approximation of τ'_w becomes $\tau'_w = \varepsilon^{-1/2} (\partial u'^i / \partial \hat{r}')|_{\hat{r}'=0} \approx (s/\varepsilon)^{1/2} \tilde{u}'_m$. This recovers to the real space using the inverse Laplace transform with the convolution theorem:

$$\tau'_w \approx \frac{1}{\sqrt{\pi \varepsilon}} \int_0^{\hat{t}'} \frac{1}{\sqrt{\hat{t}' - \xi}} \frac{du'_m(\xi)}{d\xi} d\xi \tag{A10}$$

in which $u'_m(\xi)$ is initially defined by the first of Eq.(10) for $t' \ll 1$. Substituting the first of Eq.(10) into Eq.(A10), we have

$$\tau'_w(t') \approx \frac{1}{\sqrt{\pi}} \left[\frac{16}{5} a_1 t'^{5/2} + \frac{8}{3} a_2 t'^{3/2} + 2a_3 t'^{1/2} \right] \quad \text{for } t' \ll 1 \tag{A11}$$

which is found to be identical with the asymptotic behavior of Eq.(33). The first-order approximation of the inner velocity can be obtained taking the inverse Laplace transform of Eq.(A9) as

$$u'^i(\hat{r}'; \hat{t}') \approx u'_m(\hat{t}') - \frac{\hat{r}'}{2\sqrt{\pi}} \int_0^{\hat{t}'} u'_m(\xi) \frac{\exp\left(-\dfrac{\hat{r}'^2}{4(\hat{t}' - \xi)} \right)}{(\hat{t}' - \xi)^{3/2}} d\xi. \tag{A12}$$

Here, we used the formula $\mathcal{L}^{-1}[\{2\pi^{1/2} \exp{(-cs^{1/2})}\}/c] = \exp{[-c^2/(4t')]}/t'^{3/2}$ with $c > 0$. For $t' \ll 1$, all the patterns of u'_m which are given by the first of Eq.(10) behaves like $u'_m(t') \approx a_3 t'$. Then, Eq.(Al2) is readily solved as

$$u'^i(\hat{r}';\hat{t}') \approx \varepsilon a_3 \hat{t}' - \frac{2\varepsilon a_3}{\sqrt{\pi}}\left[\left(\hat{t}' + \frac{\hat{r}'^2}{2}\right)\text{Erfc}\left(\frac{\hat{r}'}{2\sqrt{\hat{t}'}}\right) - \frac{\sqrt{\hat{t}'}}{2}\hat{r}'\exp\left(-\frac{\hat{r}'^2}{4\hat{t}'}\right)\right] \quad (A13)$$

in which Erfc indicates the complementary error function defined by Erfc $(z) = \int_z^\infty \exp{(-\xi^2)}d\xi$. For $(1 - r')^2 \ll t'$ with $t' \ll 1$, the inner velocity approximately becomes $u'^i(r'; t') \approx (2a_3/\pi^{1/2})t'^{1/2}(1 - r')$ which is found to be identical with the dominant term of Eq.(32). Note that Erfc $(z) \approx \pi^{1/2}/2 - z$ for $z \ll 1$.

In the outer domain, Eq.(A6) becomes, using the assumed outer expansion $u'^o = \sum_{n\geq0}\varepsilon^{n/2}u'^o_n$,

$$\sum_{n\geq0}\varepsilon^{n/2}\frac{\partial u'^o_n}{\partial \hat{t}'} = \frac{\partial u'_m}{\partial \hat{t}'} + 2\varepsilon\tau'_w + \varepsilon\left[\sum_{n\geq0}\varepsilon^{n/2}\frac{\partial^2 u'^o_n}{\partial r'^2} + \frac{1}{r'}\sum_{n\geq0}\varepsilon^{n/2}\frac{\partial u'^o_n}{\partial r'}\right]. \quad (A14)$$

Taking into account $\tau'_w = O(\varepsilon^{-1/2})$, the first-order solution is derives as $u'^o_0 = u'_m$. Also, the second-order approximation successively gives

$$\frac{\partial u'^o_1}{\partial \hat{t}'} = 2\sqrt{\varepsilon}\tau'_w \quad (A15)$$

in which τ'_w is given by Eq.(A10) or (All). Thus, we obtain the second-order approximation of the outer velocity as

$$u'^o(\hat{t}') \approx u'_m(\hat{t}') + \frac{2\varepsilon^{1/2}}{\sqrt{\pi}}\int_0^{\hat{t}'}d\eta\int_0^n\frac{1}{\sqrt{\eta-\xi}}\frac{du'_m(\xi)}{d\xi}d\xi \quad (A16)$$

which reduces to, for $u'_m(t') \approx a_3 t'$,

$$u'^o(t') \approx a_3 t' + \frac{8a_3}{3\sqrt{\pi}}t'^{3/2}. \quad (A17)$$

REFERENCES

1. Hino, M., Sawamoto, M. and Takasu, S., Experiments on transition to turbulence in an oscillatory pipe flow, *J. Fluid Mech.*, 1976, **75**, 193–422.

2. Iguchi, M., Urahata, I. and Ohmi, M., Turbulent slug and velocity field in the inlet region for pulsatile pipe flow, *JSME Int. J.*, 1987, **30**–261, 414–422.

3. Szymanski, P., Quelques solutions exactes des équations de l'hydrodynamique du fluide visqueux dans le cas d'un tube cylindrique, *J. Math. Pures Appl. Ser.* 9, 1932, **11**, 67–107.

4. Uchida, S., The pulsating viscous flow superposed on the steady laminar motion of incompressible fluid in a circular pipe, *ZAMP*, 1956, **VII**, 403–422.

5. Ohmi, M., Iguchi, M., Usui, T. and Minami, H., Flow pattern and frictional losses in pulsating pipe flow. Part 1 Effect of pulsating frequency on the turbulent flow pattern, *Bull. JSME*, 1980, **23**, 2013–2020.

6. Ohmi, M. and Iguchi, M., Flow pattern and frictional losses in pulsating pipe flow. Part 2 Effect of pulsating frequency on the turbulent frictional losses, *Bull. JSME*, 1980, **23**, 2021–2028.

7. Ohmi, M. and Iguchi, M., Flow pattern and frictional losses in pulsating pipe flow. Part 3 General representation of turbulent flow pattern, *Bull. JSME*, 1980, **23**, 2029–2036.

8. Ohmi, M. and Iguchi, M., Flow pattern and frictional losses in pulsating pipe flow. Part 4 General representation of turbulent frictional losses, *Bull. JSME*, 1981, **24**, 67–74.

9. Ohmi, M., Iguchi, M. and Usui, T., Flow pattern and frictional losses in pulsating pipe flow. Part 5 Wall shear stress and flow pattern in a laminar flow, *Bull. JSME*, 1981, **24**, 75–81.

10. Ohmi, M. and Iguchi, M., Flow pattern and frictional losses in pulsating pipe flow. Part 6 Frictional losses in a laminar flow, *Bull. JSME*, 1981, **24**, 1756–1763.

11. Ohmi, M. and Iguchi, M., Flow pattern and frictional losses in pulsating pipe flow. Part 7 Wall shear stress in a turbulent flow, *Bull. JSME*, 1981, **24**, 1764–1771.

12. Ohmi, M., Iguchi, M., Kakehachi, K. and Masuda, T., Transition to turbulence and velocity distribution in an oscillating pipe flow, *Bull. JSME*, 1982, **25**, 365–371.

13. Lafebvre, P. J. and White, F. M., Experiments on transition to turbulence in a constant-acceleration pipe flow, *ASME, J. Fluids Eng.*, 1989, **111**, 428–431.

14. Lafebvre, P. J. and White, F. M., Further Experiments on transition to turbulence in a constant-acceleration pipe flow, *ASME, J. Fluids Eng.*, 1991, **113**, 223–227.

15. Kurokawa, J. and Morikawa, M., Accelerated and Decelerated Flows in a Circular Pipe (1st Report, Velocity Distribution and Frictional Coefficient) (in Japanese), *Trans. JSME*, (B), 1985, **51**(467), 2076–2083.

16. Kurokawa, J. and Takagi, A., Accelerated and Decelerated Flows in a Circular Pipe (2nd Report, Transition of an Accelerated Flow) (in Japanese), *Trans. JSME*, (B), 1987, **54**(498), 302–307.

17. Moss, E. A., The Identification of Two Distinct Laminar to Turbulent Transition Modes in Pipe Flows Accelerated from Rest, *Experiments in Fluids*, 1989, **7**, 271–274.

18. Greenblatt, D. and Moss, E. A., Rapid transition to turbulence in pipe flows accelerated from rest, *ASME, J. Fluids Eng.*, 2003, **125**, 1072–1075.

19. Koppel, T. and Ainola, L., Identification of transition to turbulence in a highly accelerated start-up pipe flow, *ASME, J. Fluids Eng.*, 2006, **128**, 680–686.

20. Nishihara, K., Knisely, C. W., Nakahata, Y., Wada, I. and Iguchi, M., Control of transition to turbulence in constant-acceleration square duct flow (in Japanese), *J. JSEM*, 2008, **8**(3), 213–218.

21. Nishihara, K., Knisely, C. W., Nakahata, Y., Wada, I. and Iguchi, M., Transition to turbulence in constant velocity pipe flow after initial constant-acceleration, *J. JSEM*, 2009, **9**, 30–35.

22. Das, D. and Arakeri, J. H., Transition of unsteady velocity profiles with reverse flow, *J. Fluid Mech.*, 1998, **374**, 251–283.

23. Das, D. and Arakeri, J. H., Unsteady laminar duct flow with a given volume flow rate variation, *ASME, J. Appl. Mech.*, 2000, **67**, 274–281.

24. Nishihara, K., Nakahata, Y., Ueda, Y., Knisely, C. W., Sasaki, Y. and Iguchi, M., Effect of initial acceleration history on transition to turbulence in pipe flow, Submitted to *J. JSEM*.

25. Ghidaoui, M. S. and Kolyshkin, A. A., A quasi-steady approach to the instability of time-dependent flows in pipes," *J. Fluid Mech.,* 2002, 465, 301–330.

26. Abramowitz, M. and Stegun, L. A., *Handbook of Mathematical Functions with Formulas, Graphs, and Mathematical Tables,* Dover, 1965.

27. Van Dyke, M., *Perturbation methods in fluid mechanics*, Parabolic Press, Stanford, 1975.

28. The zeros y_n (n = 1, 2, $\cdots$, 10) of $J_2(y)$ used are listed as follows: y_1 = 5.1356, y_2 = 8.4172, y_3 = 11.6198, y_4 = 14.7959, y_5 = 17.9598, y_6 = 21.1169, y_7 = 24.2700, y_8 = 27.4205, y_9 = 30.5691, y_{10} = 33.7165. For a large n, the zero y_n is described as $y_n \sim \beta = 15/(8\beta) - 4860/[3(8\beta)^3] - 4471200/[15(8\beta)^5] - 7844040000/[105(8\beta)^7]$, where $\beta = (s + 3/4)\pi$.